

A reduced 3D-0D FSI model of the aortic valve including leaflets curvature

Ivan Fumagalli

MOX - Department of Mathematics, Politecnico di Milano, Milan, Italy

Abstract

In the present work, we propose a novel lumped-parameter model for the description of the aortic valve dynamics, including elastic effects associated to the leaflets' curvature. The introduction of a lumped-parameter model based on momentum balance entails an easier calibration of the parameter models, that are instead typically numerous in phenomenological-based models. This model is coupled with 3D Navier-Stokes equations describing the blood flow, where the valve surface is represented by a resistive method, and valve leaflets velocity is taken into consideration. The resulting reduced fluid-structure interaction problem has a computational cost that is comparable with the solution of a prescribed-motion fluid dynamics problem. A SUPG-PSPG stabilized finite element scheme is adopted for the discretization of the coupled problem, and the computational results show the suitability of the system in representing the leaflets motion, the blood flow in the ascending aorta, and the pressure jump across the leaflets.

1 Introduction

The main role of cardiac valves in the hemodynamics of the heart and proximal vessels is to prevent a reverse flow, but their shape and motion also help in reducing blood stagnation, improving the chamber washout, orienting the jets and affecting the coherent vortex structures of the flow. Because of the relevance of such components, many cardiac pathologies are directly related or at least entail valvular abnormal conditions, such as calcification, stenosis, regurgitation, and anatomical defects interesting the leaflets or the subvalvular apparatus.

For all these reasons, a computational model aiming at reproducing and analyzing cardiac hemodynamics requires to include valves geometry and dynamics. Different valve mechanical models have been proposed in the literature, focusing on different features of the leaflets tissue, but the discussion is still open about the accuracy of these models to represent their actual behavior, due to the difficulties of obtaining in vivo measurements. Some of the proposed models present a very detailed anatomy and physiology, including the inhomogeneities and the fibers in the leaflets [MPH⁺13, Mar15] or a mechanical coupling with the subvalvular apparatus and the proximal vessels, such as [KC90, RMK14, SCM⁺07, Bel69, MDA13] and many others. In order to use such rich models

to investigate hemodynamics, the solution of a three-dimensional fluid-structure interaction (FSI) problem is required. Several techniques have been employed to account for the valves motion in the blood pool and its coupling with hemodynamics, either in a boundary-fitting setting or from a Eulerian standpoint: the Arbitrary Lagrangian Eulerian framework [CLC04, JDS96, ESH14, BQČG17], the CUTFEM and XFEM methods [AFFL16, HLZ15, BF14, GW10, MPGW10, MLLR15, GW08, FVZ18, ZVF18], the immersed boundary [Pes72, GLMP09, Gri12, HKB⁺14, WZK⁺18, LLF⁺06, YYKZ18, VLS⁺13, GS10, BGS08, BGS10] and the fictitious domain approach [GPP97, vLAvdV06, DSGB08, AGPT09, BHK⁺11, KHS⁺15, DHPSB03, SDHBVdV04, MYWD07], or other methods such as chimera [GLSY05, MCE⁺14, ZSJ09] and space-time finite elements [HH88, TS07, TTTS18]. The common denominator of all these methods is that they require a full 3D (or at least 2D) representation of the valve geometry and of its mechanics solver, thus entailing a significantly increased computational cost with respect to imposed-displacement hemodynamics.

Aiming at providing reliable information on the valve dynamics with little computational overhead, lumped-parameter models have been introduced for valve dynamics. Most of these models, e.g. [KS06, BF⁺10, RSA⁺20a], typically represent the valve hemodynamical effects by means of a phenomenological relationship between the pressure jump across the leaflets and the flowrate passing through them. However, since the single parameters appearing in the equations do not have a precisely quantifiable physical meaning, the calibration of the model may be quite cumbersome and relatively highly dependent on the specific application of interest. Other works, on the other hand derive their reduced model from a momentum balance at the leaflets. Up to the authors' knowledge, this approach has been first adopted in [DP15], where the inertia and stiffness of the leaflets are neglected. In a more recent work [SZRM20], however, these properties are considered in a linear ordinary differential equation.

We introduce a novel lumped-parameter structure model for the aortic valve, with the aim of enriching the description of the valve dynamics while preserving a low computational effort. We derive our model from the balance of forces at the leaflet, relating the elasticity of the leaflets to its curvature. This approach allows to automatically account for the specific valve geometry and to relate it directly with the flow-induced forces to which the leaflets are subject.

Based on this mechanical model, a reduced 3D-0D fluid-structure interaction (FSI) system is introduced, modeling the interplay between the three-dimensional blood flow in the ascending aorta and the aortic valve dynamics. Blood dynamics is described by incompressible Navier-Stokes equations, and the hemodynamics effect of the valve's kinematics are accounted for by the Resistive Immersed Implicit Surface method (RIIS) introduced in [FFDQ17]. This method, based on the Resistive Immersed Surface (RIS) method introduced in [FGM08] and applied to cardiac valves in [AHSG12], lays in the aforementioned immersed-boundary / fictitious-domain framework, and it consists in the addition of a penalty term to the fluid momentum equation. It is characterized by a fundamentally negligible computational overhead in CFD simulations, and its suitability for the description of hemodynamics effect of valves has been shown in the case of the aortic valve in [FFDQ17] and in a pathological condition involving the mitral valve in [FFV⁺20].

The structure of the present work is the following. In Section 2 we introduce the FSI mathematical model, made of the novel lumped-parameter structural

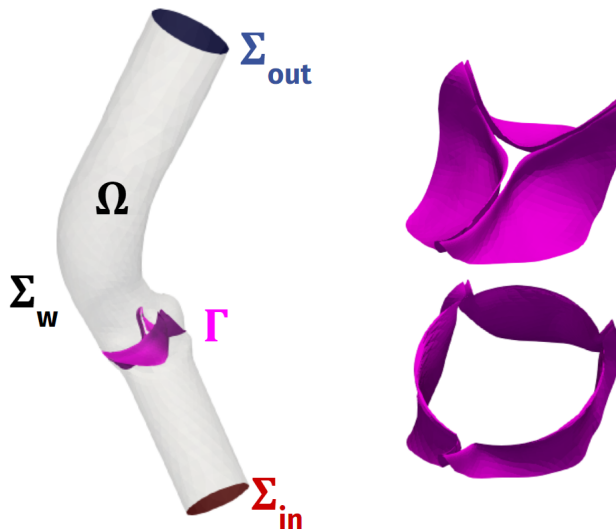


Figure 1: Computational domain Ω with its boundaries (left) and the immersed valve Γ in purple; closed (top right) and open (bottom right) configuration of the aortic valve.

model of the aortic valve, the blood flow equations including the RIIS representation of the leaflets, and the coupling between the two systems. The numerical approximation of the reduced FSI problem and the scheme for its solution are described in Section 3. Then, computational results are presented in Section 4, displaying the suitability of the presented model to describe the physical system of interest.

2 Mathematical models and methods

We introduce a reduced model representing the fluid-structure interaction system of blood flow in the aorta and the aortic valve leaflets. In Section 2.1, we introduce the fluid dynamics system, with the valve effects modeled by a resistive method [FFDQ17]. Then, a reduced structure model for valve dynamics is derived in Section 2.2, considering the external forces induced on the leaflets by the surrounding blood, and the FSI coupling is presented in Section 2.3.

2.1 Fluid model and RIIS method

We model blood as an incompressible, Newtonian fluid with uniform density ρ and viscosity μ , contained in the domain Ω represented in Fig. 1. The effects of the valve on the fluid dynamics are accounted for by the Resistive Immersed Implicit Surface (RIIS) method, introduced in [FFDQ17] and employed in [FFV⁺20] in a clinical context. This method, based on the Resistive Immersed Surface (RIS) approach proposed in [FGM08, AGPT09, AHSG12], consists in the introduction of an additional penalty term in the fluid momentum equation, thus weakly imposing the kinematic condition at the surface representing the valve.

According to the RIIS method, the geometry of the moving valve Γ_t is represented as a surface immersed in the fluid domain Ω , implicitly described at each time t by a level-set function $\varphi_t : \Omega \rightarrow \mathbb{R}$, as

$$\Gamma_t = \{\mathbf{x} \in \Omega : \varphi_t(\mathbf{x}) = 0\}.$$

The function φ_t is assumed to be a signed distance function, namely to fulfill $|\nabla\varphi_t| = 1$, for any t . A smeared Dirac delta function $\delta_{t,\varepsilon} : \Omega \rightarrow [0, +\infty)$ is then introduced, to approximate the Dirac distribution – rigorously, the codimension-1 Hausdorff measure – with support on the surface Γ_t , as follows:

$$\delta_{t,\varepsilon}(\mathbf{x}) = \begin{cases} \frac{1+\cos(\pi\varphi_t(\mathbf{x})/\varepsilon)}{2\varepsilon} & \text{if } |\varphi_t(\mathbf{x})| \leq \varepsilon, \\ 0 & \text{if } |\varphi_t(\mathbf{x})| > \varepsilon, \end{cases}$$

where the half-thickness ε is the smoothing parameter.

In these settings, the velocity \mathbf{u} and pressure p of the blood satisfy the following formulation of the Navier-Stokes equations:

$$\begin{cases} \partial_t \mathbf{u} + \rho \mathbf{u} \cdot \nabla \mathbf{u} - \nabla \cdot \boldsymbol{\sigma} + \frac{R}{\varepsilon} (\mathbf{u} - \mathbf{u}_\Gamma) \delta_{t,\varepsilon} = \mathbf{0} & \text{in } \Omega, t \in (0, T], \\ \nabla \cdot \mathbf{u} = 0 & \text{in } \Omega, t \in (0, T], \\ \mathbf{u} = \mathbf{0} & \text{on } \Sigma_w, t \in (0, T], \\ \boldsymbol{\sigma} \mathbf{n} = p_{\text{in}} \mathbf{n}, & \text{on } \Sigma_{\text{in}}, t \in (0, T], \\ \boldsymbol{\sigma} \mathbf{n} = p_{\text{out}} \mathbf{n}, & \text{on } \Sigma_{\text{out}}, t \in (0, T], \\ \mathbf{u} = \mathbf{0} & \text{in } \Omega, t = 0, \end{cases} \quad (1)$$

where $\boldsymbol{\sigma} = 2\mu D(\mathbf{u}) - pI = \mu(\nabla \mathbf{u} + \nabla \mathbf{u}^T) - pI$ is the fluid stress tensor, R is the resistance of the RIIS term – acting as a penalty parameter – and \mathbf{u}_Γ is the velocity of the valve, which constitutes a data for the fluid problem and will be discussed in the following sections. Regarding boundary conditions, $p_{\text{in}}, p_{\text{out}}$ are the pressure values imposed at the inflow and outflow boundaries $\Sigma_{\text{in}}, \Sigma_{\text{out}}$, respectively, while the boundary Σ_w represents the aortic wall.

2.2 Lumped-parameters mechanical model

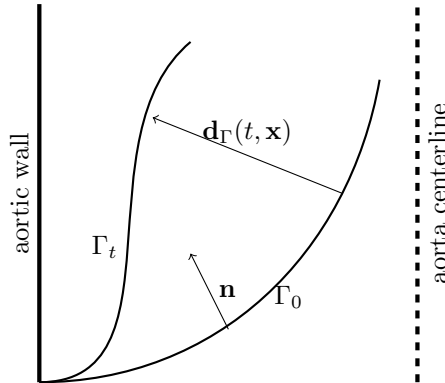


Figure 2: Schematic representation of a leaflet section and its motion.

In order to provide the configuration and the velocity of the valve, represented by φ_t and \mathbf{u}_Γ in the fluid problem (1), a structural model would be required for the deformation of the surface Γ_t . This section is devoted to the derivation of a reduced, lumped-parameters model realistically describing the main features of cardiac valve dynamics. The approach differs from the one proposed in [SZRM20] in that the elastic terms are related to the curvature of the leaflet, thus including additional geometrical information in the model.

Let $\mathbf{d}_\Gamma : [0, T] \times \widehat{\Gamma} \rightarrow \mathbb{R}^3$ denote the displacement of the leaflet with respect to its reference configuration $\Gamma_0 = \widehat{\Gamma}$, namely we can represent the current configuration Γ_t as

$$\Gamma_t = \{\mathbf{x} \in \mathbb{R}^3 : \mathbf{x} = \mathbf{T}_t(\widehat{\mathbf{x}}) = \widehat{\mathbf{x}} + \mathbf{d}_\Gamma(t, \widehat{\mathbf{x}}) \text{ for some } \widehat{\mathbf{x}} \in \widehat{\Gamma}\},$$

as schematically displayed in Fig. 2.

We assume that at each time t , each point $\mathbf{x} \in \Gamma_t$ of the leaflet is subject to an external force $\mathbf{f}(t, \mathbf{x})$ due to the surrounding fluid and to an elastic force related to the leaflet curvature $H(\mathbf{x})$, and that the valve motion can be affected by some damping effect. Regarding the curvature-induced elastic force, we assume that it acts only normally to the surface, similarly to what happens in free-surface tension. Moreover, since it is generally observed that the resting state of the aortic valve is its closed configuration, we impose this elastic force to vanish on $\widehat{\Gamma}$.

In accordance to these assumptions, a local force balance can be formulated as follows:

$$\rho_\Gamma \ddot{\mathbf{x}} + \beta \rho_\Gamma \dot{\mathbf{x}} = \mathbf{f}(t, \mathbf{x}) - \gamma [H(\mathbf{x}) - \widehat{H}(\widehat{\mathbf{x}})] \mathbf{n}_\Gamma(\mathbf{x}), \quad (2)$$

where ρ_Γ is the *surface* density of the valve, β is a damping coefficient, γ is an elasticity coefficient, and \mathbf{n}_Γ is the normal to the surface Γ_t . The function $\widehat{H}(\widehat{\mathbf{x}})$ denotes the total curvature of the surface $\widehat{\Gamma}$ in the position $\widehat{\mathbf{x}} = \mathbf{T}_t^{-1}(\mathbf{x})$ corresponding to \mathbf{x} . For simplicity, and in accordance to the common practice for biological tissues, in the present work we consider the valve leaflets to have the same density as blood. Thus, $\rho_\Gamma = 2\varepsilon\rho$, where ε denotes the semi-thickness of the leaflet: by RIIS representation, we have the following consistency formula

$$\int_{\Gamma_t} \rho_\Gamma d\Gamma \simeq \int_{\Omega} 2\varepsilon\rho\delta_{t,\varepsilon} d\Omega = \rho 2\varepsilon|\Gamma_t|.$$

It is worth to point out that the parameter ρ_Γ can be tuned to different values – without loss of generality – in order to account for different inertial properties of the leaflets.

Aiming at reducing equation (2) to a 0D model, we assume that \mathbf{d}_Γ can be decomposed as

$$\mathbf{d}_\Gamma(t, \widehat{\mathbf{x}}) = c(t)\mathbf{g}(\widehat{\mathbf{x}}),$$

where $\mathbf{g} : \widehat{\Gamma} \rightarrow \mathbb{R}^3$ is known, whilst $c : [0, T] \rightarrow \mathbb{R}$ has to be modeled. In these settings, the local balance (2) can be re-written as

$$[\ddot{c}(t) + \beta\dot{c}(t)] \rho_\Gamma \mathbf{g}(\mathbf{T}_t^{-1}(\mathbf{x})) = \mathbf{f}(t, \mathbf{x}) - \gamma [H(\mathbf{x}) - \widehat{H}(\mathbf{T}_t^{-1}(\mathbf{x}))] \mathbf{n}_\Gamma(\mathbf{x}).$$

Taking the component along $\mathbf{n}_\Gamma(\mathbf{x})$ and integrating over Γ_t , we obtain the following ordinary differential equation for c :

$$\ddot{c} + \beta\dot{c} = \frac{\int_{\Gamma_t} \mathbf{f}(t, \mathbf{x}) \cdot \mathbf{n}_\Gamma(\mathbf{x}) d\mathbf{x} - \gamma \int_{\Gamma_t} [H(\mathbf{x}) - \widehat{H}(\mathbf{T}_t^{-1}(\mathbf{x}))] d\mathbf{x}}{\int_{\Gamma_t} \rho_\Gamma \mathbf{g}(\mathbf{T}_t^{-1}(\mathbf{x})) \cdot \mathbf{n}_\Gamma(\mathbf{x}) d\mathbf{x}}. \quad (3)$$

This equation can be completed by proper initial conditions on $c(0)$ and $\dot{c}(0)$, depending on the application of interest.

2.3 Coupling of the fluid and structure models

The 3D fluid model described in Section 2.1 and the 0D valve model introduced in Section 2.2 can be coupled in a reduced FSI model. This consists in providing the fluid-to-valve stress distribution \mathbf{f} appearing in equation (3) in terms of \mathbf{u} , p and the RIIS-related quantities, and in reinterpreting the RIIS signed distance function φ_t and the leaflet velocity \mathbf{u}_Γ appearing in (1) as functions of c and \mathbf{g} . To this aim, we introduce some additional notation related to the representation of the immersed surface Γ_t . Being φ_t a signed distance function, the domain Ω can be partitioned into two regions

$$\Omega_t^+ = \{\mathbf{x} \in \Omega: \varphi_t(\mathbf{x}) \geq 0\}, \quad \Omega_t^- = \{\mathbf{x} \in \Omega: \varphi_t(\mathbf{x}) \leq 0\},$$

whose intersection is Γ_t . Accordingly, any function f defined over Ω can be decomposed as $f = f^+ + f^-$, where $f^\pm = f|_{\Omega^\pm}$. Moreover, the function φ_t allows to define $\tilde{\mathbf{n}}_\Gamma$ and \tilde{H} , that are the extensions to the whole domain Ω of the surface normal \mathbf{n}_Γ and its curvature H , respectively:

$$\begin{aligned} \tilde{\mathbf{n}}_\Gamma &= \frac{\nabla \varphi_t}{|\nabla \varphi_t|}, \\ \tilde{H} &= -\operatorname{div} \tilde{\mathbf{n}}_\Gamma = -\frac{\Delta \varphi_t}{|\nabla \varphi_t|} + \frac{\nabla^2 \varphi_t - \nabla \varphi_t \otimes \nabla \varphi_t}{|\nabla \varphi_t|^3}. \end{aligned} \quad (4)$$

These quantities are actual extensions of the normal vector and curvature, since $\tilde{\mathbf{n}}_\Gamma|_\Gamma = \mathbf{n}_\Gamma$, $\tilde{H}|_\Gamma = H$. We remark that $\tilde{\mathbf{n}}_\Gamma$ is such that it does not change its verse when passing through Γ_t .

Remark 1 (Normalization). We point out that in the definitions (4), we did not make the common assumption that $|\nabla \varphi_t| \equiv 1$. Indeed, although such an assumption holds in the neighborhood of internal points of Γ_t , its validity is broken near $\partial\Gamma_t$, where φ_t is not continuous. Moreover, this definition of $\tilde{\mathbf{n}}_\Gamma$ ensures that the normal has unit magnitude also at the discrete level.

Regarding the function \mathbf{g} , which is defined only on $\hat{\Gamma}$, we can define its extension to any location $\mathbf{y} \in \Omega$ by taking the value assumed by \mathbf{g} at the projection $\hat{\mathbf{y}} \in \hat{\Gamma}$ of \mathbf{y} onto $\hat{\Gamma}$. A similar extension can be defined also for \tilde{H} .

The quantities defined above represent the geometric description of the valve leaflets: we now introduce its kinematics and dynamics.

Regarding the kinematic description of the surface represented in the RIIS fashion, a definition of the surface velocity \mathbf{u}_Γ is required. For the purposes of the present section, resorting to the level-set properties of the function φ_t (cf. [OF01, FFDQ17]), we can define the leaflet velocity \mathbf{u}_Γ as

$$\mathbf{u}_\Gamma = -\partial_t \varphi_t \frac{\nabla \varphi_t}{|\nabla \varphi_t|}. \quad (5)$$

An operative and more concrete definition of \mathbf{u}_Γ will be provided in the discrete settings, in Section 3.

The forces exerted by the fluid on the valve are related to the stress jump across Γ_t , thus

$$\mathbf{f} = [\boldsymbol{\sigma}\mathbf{n}_\Gamma]_{\Gamma_t} = \boldsymbol{\sigma}^+|_{\Gamma_t}\mathbf{n}_\Gamma - \boldsymbol{\sigma}^-|_{\Gamma_t}\mathbf{n}_\Gamma.$$

Considering the surface smearing introduced by the smooth Dirac delta $\delta_{\Gamma,\varepsilon}$ and the definitions (4), the integral term related to \mathbf{f} that appears in (3) can be approximated as follows:

$$\int_{\Gamma_t} \mathbf{f} \cdot \mathbf{n}_\Gamma \simeq \int_{\Omega} \left(\boldsymbol{\sigma}\tilde{\mathbf{n}}_\Gamma \cdot \tilde{\mathbf{n}}_\Gamma \delta_{\Gamma,\varepsilon}^+ - \boldsymbol{\sigma}\tilde{\mathbf{n}}_\Gamma \cdot \tilde{\mathbf{n}}_\Gamma \delta_{\Gamma,\varepsilon}^- \right). \quad (6)$$

Analogously, the other integrals of (3) can be approximated as follows:

$$\begin{aligned} \int_{\Gamma_t} \rho_\Gamma (\mathbf{g} \circ \mathbf{T}_t^{-1}) \cdot \mathbf{n}_\Gamma &\simeq \int_{\Omega} \rho_\Gamma (\mathbf{g} \circ \mathbf{T}_t^{-1}) \cdot \tilde{\mathbf{n}}_\Gamma \delta_{\Gamma,\varepsilon}, \\ -\gamma \int_{\Gamma_t} \left(H - \widehat{H} \circ \mathbf{T}_t^{-1} \right) &\simeq -\gamma \int_{\Omega} \left(\widetilde{H} - \widehat{H} \right) \delta_{\Gamma,\varepsilon}, \end{aligned} \quad (7)$$

with \widehat{H} denoting the RIIS representation of the pulled-back curvature $\widehat{H} \circ \mathbf{T}_t^{-1}$.

Remark 2 (Pressure jump). Notice that, since $|\tilde{\mathbf{n}}_\Gamma| \equiv 1$, if the strain component of the normal stress is assumed to be negligible w.r.t. the pressure term, the integral force in (6) gets down to

$$\int_{\Gamma_t} \mathbf{f} \cdot \mathbf{n}_\Gamma \simeq \int_{\Omega} \left(p \delta_{\Gamma,\varepsilon}^+ - p \delta_{\Gamma,\varepsilon}^- \right),$$

in accordance with other reduced models, such as [KS06, BF⁺10, SZRM20, DP15], which are based on the pressure jump across the valve.

The definitions and approximations presented in this section allow to exchange information between the 3D fluid model and the 0D structure model. The next section is devoted to the time and space discretization of the coupled model, and to devising a solution strategy.

3 Numerical approximation

In the present section, the space and time discretization of the coupled 3D-0D FSI model is presented. We introduce a uniform partition of the time interval $[0, T]$ with step-size Δt and nodes $\{t^n\}_{n=0}^N$. Accordingly, the time-discrete counterparts of all quantities, evaluated at time t^n , will be denoted by a superscript \cdot^n . For the space discretization, we introduce a hexahedral mesh \mathcal{T}_h for the domain Ω , and the Finite Element (FE) space

$$X_h^r = \{v_h \in C^0(\overline{\Omega}): v_h|_T \in \mathbb{Q}^r(T), \forall T \in \mathcal{T}_h\},$$

where \mathbb{Q}^r denotes the space of polynomials of degree r w.r.t. each space coordinate. The velocity and pressure discrete spaces are thus defined as $V_h^r = \{\mathbf{v}_h \in [X_h^r]^3: \mathbf{v}_h = \mathbf{0} \text{ on } \Sigma_w\}$ and $Q_h^r = X_h^r$.

For the approximation of the fluid problem (1), we adopt a semi-implicit BDF-FE scheme of order σ like the one presented in [FFDQ17], where the same polynomial degree r is considered for V_h^r and Q_h^r , together with a SUPG-PSPG stabilization with VMS-inspired coefficients [FD15, BCC⁺07].

The resulting numerical method reads as follows:
 Given $\mathbf{u}_h^n, n = 0, \dots, \sigma - 1$, for each $n = \sigma, \dots, N$, find \mathbf{u}_h^n, p_h^n such that

$$\begin{aligned} & \left(\rho \frac{\alpha_\sigma \mathbf{u}_h^n - \mathbf{u}_h^{n, \text{BDF}\sigma}}{\Delta t}, \mathbf{v}_h \right) + \bar{a}^n(\mathbf{u}_h^n, \mathbf{v}_h) + c(\mathbf{u}_h^{n, \sigma}, \mathbf{u}_h^n, \mathbf{v}_h) \\ & + b(\mathbf{v}_h, p_h^n) - b(\mathbf{u}_h^n, q_h) + \sum_{T \in \mathcal{T}_h} (\tau_M^{n, \sigma} \mathbf{r}_M^n(\mathbf{u}_h^n, p_h^n), \rho \mathbf{u}_h^{n, \sigma} \cdot \nabla \mathbf{v}_h + \nabla q_h)_T \\ & + \sum_{T \in \mathcal{T}_h} (\tau_C^{n, \sigma} r_C^n(\mathbf{u}_h^n), \nabla \cdot \mathbf{v}_h)_T = F(\mathbf{v}_h) \end{aligned} \quad (8)$$

for all $\mathbf{v}_h \in V_h, q_h \in Q_h$, where (\cdot, \cdot) and $(\cdot, \cdot)_T$ denote the L^2 inner product over Ω and a mesh element T , respectively, $\alpha_\sigma, \mathbf{u}_h^{n, \text{BDF}\sigma}$ and the extrapolated velocity $\mathbf{u}_h^{n, \sigma}$ depend on the order σ of the BDF scheme [FD15], the BDF quantities $\mathbf{r}_M^n, r_C^n, \tau_M^{n, \sigma}, \tau_C^{n, \sigma}$ are defined as

$$\begin{aligned} \mathbf{r}_M^n(\mathbf{u}_h^n, p_h^n) &= \rho \frac{\alpha_\sigma \mathbf{u}_h^n - \mathbf{u}_h^{n, \text{BDF}\sigma}}{\Delta t} - \mu \Delta \mathbf{u}_h^n + \rho \mathbf{u}_h^{n, \sigma} \cdot \nabla \mathbf{u}_h^n + \nabla p_h^n + \frac{R}{\varepsilon} \delta_\varepsilon^n (\mathbf{u}_h^n - \mathbf{u}_\Gamma^n), \\ r_C^n(\mathbf{u}_h^n) &= \nabla \cdot \mathbf{u}_h^n, \\ \tau_M^{n, \sigma} &= \left(\frac{\rho^2 \alpha_\sigma^2}{\Delta t^2} + \rho^2 \mathbf{u}_h^{n, \sigma} \cdot G \mathbf{u}_h^{n, \sigma} + C_r \mu^2 G : G + \frac{R^2}{\varepsilon^2} (\delta_\varepsilon^n)^2 \right)^{-1/2}, \\ \tau_C^{n, \sigma} &= (\tau_M^{n, \sigma} \mathbf{g} \cdot \mathbf{g})^{-1}, \end{aligned}$$

and the variational forms are

$$\begin{aligned} \bar{a}^n(\mathbf{u}, \mathbf{v}) &= (\mu D(\mathbf{u}), \nabla \mathbf{v}) + \left(\frac{R}{\varepsilon} \mathbf{u} \delta_\varepsilon^n, \mathbf{v} \right), \\ b(\mathbf{v}, q) &= -(\text{div} \mathbf{v}, q), \\ c(\mathbf{w}, \mathbf{u}, \mathbf{v}) &= (\mathbf{w} \cdot \nabla \mathbf{u}, \mathbf{v}), \\ F(\mathbf{v}) &= \int_{\Sigma_{\text{in}}} p_{\text{in}} \mathbf{n} \cdot \mathbf{v} + \int_{\Sigma_{\text{out}}} p_{\text{out}} \mathbf{n} \cdot \mathbf{v} - \left(\frac{R}{\varepsilon} \mathbf{u}_\Gamma^n \delta_\varepsilon^n, \mathbf{v} \right). \end{aligned}$$

The quantities G and \mathbf{g} appearing above are metric tensors, depending on the element map $\mathbf{M}_T : \hat{T} \rightarrow T$, for $T \in \mathcal{T}_h$, mapping the reference element \hat{T} to the current one T [TS03].

Regarding the geometric quantities describing the valve, we hinge upon a FE description, but we do not need all of them to actually belong to a FE space, since they are going to appear only inside of integrals. In particular, the distance function is approximated by $\varphi_h^n \in X_h^s$ at each time t^n – with a polynomial degree $s \geq 2$ that is in general different from r – and $\delta_{\varepsilon, h}^n$ is defined accordingly. It is worth to remark at this point that, in order for $\delta_{\varepsilon, h}^n$ to be correctly resolved by the mesh, the half-thickness ε must be at least 1.5 times larger than h [FFDQ17].

Denoting by $\{\psi_\ell\}_{\ell=1}^{N_h^s}$ the basis functions spanning X_h^s , the distance function reads $\varphi_h^n = \sum_{\ell=1}^{N_h^s} \varphi_\ell^n \psi_\ell$, and the leaflet's extended normal and curvature are

then defined as follows:

$$\begin{aligned}
\tilde{\mathbf{n}}_{\Gamma,h}^n &= \frac{\sum_{\ell=1}^{N_h^s} \varphi_\ell^n \nabla \psi_\ell}{\left| \sum_{\ell=1}^{N_h^s} \varphi_\ell^n \nabla \psi_\ell \right|}, \\
\tilde{H}_{\Gamma,h}^n &= \operatorname{div} \tilde{\mathbf{n}}_{\Gamma,h}^n \\
&= \frac{\sum_{\ell=1}^{N_h^s} \varphi_\ell^n \Delta \psi_\ell}{\left| \sum_{\ell=1}^{N_h^s} \varphi_\ell^n \nabla \psi_\ell \right|} - \frac{\sum_{\ell=1}^{N_h^s} \varphi_\ell^n \nabla^2 \psi_\ell : \left(\sum_{\ell=1}^{N_h^s} \varphi_\ell^n \nabla \psi_\ell \otimes \sum_{\ell=1}^{N_h^s} \varphi_\ell^n \nabla \psi_\ell \right)}{\left| \sum_{\ell=1}^{N_h^s} \varphi_\ell^n \nabla \psi_\ell \right|^3} \\
&= \frac{\sum_{\ell=1}^{N_h^s} \varphi_\ell^n \Delta \psi_\ell}{\left| \sum_{\ell=1}^{N_h^s} \varphi_\ell^n \nabla \psi_\ell \right|} - \frac{\sum_{\ell,m,k=1}^{N_h^s} \varphi_\ell^n \varphi_m^n \varphi_k^n \nabla^2 \psi_\ell : (\nabla \psi_m \otimes \nabla \psi_k)}{\left| \sum_{\ell=1}^{N_h^s} \varphi_\ell^n \nabla \psi_\ell \right|^3}
\end{aligned} \tag{9}$$

We point out that, since both these quantities appear in the valve model only inside integrals of the form (6)-(7), we can use directly the expressions (9), without the need of a projection onto a finite element space.

In order to represent the leaflet velocity at the discrete level, we exploit fact that the its displacement on time via the opening coefficient $c(t)$. From a first-order approximation of (5), we introduce

$$\mathbf{u}_{\Gamma,h}^n = \frac{c^n - c^{n-1}}{\Delta t} \tilde{\mathbf{n}}_{\Gamma,h}^n. \tag{10}$$

Regarding the solution of the ODE equation (3) describing the valve dynamics, an explicit, fourth-order Runge-Kutta method. The fluid and structure models are then weakly coupled at each time-step, as described in the following scheme:

Algorithm 1: Solution scheme for the 3D-0D FSI model

Given $\mathbf{u}_h^n, p_h^n, c^n$ for $n = 0, \dots, \sigma - 1$, and computed the functions $\varphi^n, \tilde{\mathbf{n}}_{\Gamma}^n, \tilde{H}^n$ corresponding to the surface Γ^n , for $n = 0, \dots, \sigma - 1$,

for $n = \sigma$ **to** N **do**

Compute the integrals that make up (3), in terms of

$\mathbf{u}_h^{n-1}, p_h^{n-1}, \Gamma^{n-1}, \varphi^{n-1}$;

Find c^n by advancing the 0D equation (3) with a step of an explicit fourth-order Runge-Kutta method;

Create the immersed surface Γ^n moving the previous configuration Γ^{n-1} by $\mathbf{d}_{\Gamma}^n = (c^n - c^{n-1})\mathbf{g}$;

Compute the new signed distance function φ^n w.r.t. Γ^n and assemble the normal and curvature fields $\tilde{\mathbf{n}}_{\Gamma}^n$ and \tilde{H}^n ;

Compute the leaflet velocity $\mathbf{u}_{\Gamma}^n = \frac{\varphi^n - \varphi^{n-1}}{\Delta t} \tilde{\mathbf{n}}_{\Gamma}^n$;

Find $(\mathbf{u}_h^n, p_h^n) \in V_h^r \times Q_h^r$ by solving the linear problem (8).

end

This solution scheme has been implemented within life^x [lif], a high-performance parallel C++ library for the solution of multi-physics problems based on the deal.II finite element core [dea].

ρ $\left[\frac{\text{kg}}{\text{m}^3}\right]$	μ $\left[\frac{\text{kg}}{\text{m s}}\right]$	R $\left[\frac{\text{kg}}{\text{m s}}\right]$	ε [m]	β [s ⁻¹]	γ $\left[\frac{\text{N}}{\text{m}}\right]$	T_S [s]	Δt [s]
10^3	$3.5 \cdot 10^{-3}$	10000	10^{-3}	2	0.2	0.4	$2 \cdot 10^{-4}$

Table 1: Physical and numerical parameters.

4 Numerical simulations

We show the suitability of the proposed reduced 3D-0D FSI model in describing blood and valve dynamics in the ascending aorta. Both the geometry of the domain Ω and of the closed valve leaflets Γ are taken from Zygote [Zyg14], an accurate model of the physiological heart derived from scan acquisitions. A proper opening field \mathbf{g} has been introduced on the leaflets, so that the surface $\{\mathbf{x} = \hat{\mathbf{x}} + \mathbf{g}(\hat{\mathbf{x}}), \hat{\mathbf{x}} \in \hat{\Gamma}\}$ represents the open valve configuration, with a maximum orifice area of 3 cm² laying the physiological range.

The domain is discretized by a hexahedral mesh of about 100K elements including artificial flow extensions at both inlet and outlet. The elements size range from 2 mm in the flow extensions to 0.5 mm in the Valsalva sinuses. Blood velocity and pressure are both discretized with \mathbb{Q}_1 finite elements, and a BDF order of 1 is chosen. The other physical and numerical parameters of the system are reported in Table 1.

Regarding boundary conditions at the inlet and outlet sections of the domain we impose the time-dependent normal stresses $p_{\text{in}}(t), p_{\text{out}}(t)$ displayed in Fig. 3, obtained from the lumped circulation presented in [RSA⁺20a, RSA⁺20b] after proper calibration in order to be consistent with physiological pressures as reported in Wiggers diagrams [Wig23]. We focus on the opening phase, up to the inversion of the pressure jump at $t = 0.2\text{s}$.

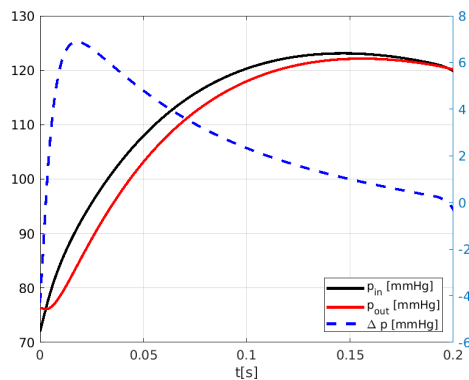


Figure 3: Pressure boundary conditions.

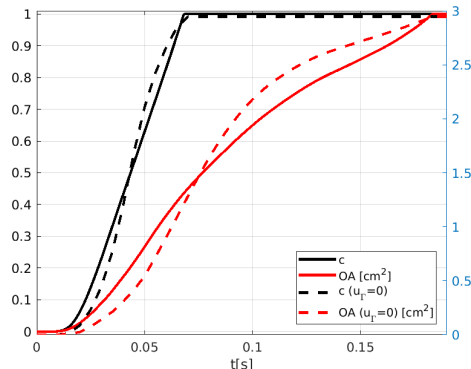


Figure 4: Opening coefficient c (left axis) and orifice area OA (right axis) under physiological pressure conditions. The case $\mathbf{u}_\Gamma = \mathbf{0}$ is discussed in Section 4.2.

4.1 Physiological valve opening

As we can see from Fig. 4, the opening valve dynamics is characterized by different phases:

- i) The leaflets remain closed until a minimal transvalvular pressure jump of about 5 mmHg is developed.
- ii) Then, they rapidly open up to their fully open position, in a timespan of 61 ms, in accordance with the measures of 76 ± 30 ms reported in [HHB⁺03].
- iii) In most part of the systole the valve remains in its fully open configuration, while the pressure jump progressively decreases.

The evolution of the blood flow during this systolic ejection is reported in Fig. 5. In the early stages of the simulation, while the valve is closed, the whole pressure gradient is concentrated across the valve. Then, the opening of the valve is accompanied by a progressive development of the typical jet flow through the aortic orifice, and much smaller pressure differences can be appreciated.

In order to better appreciate the role of pressure in the valve dynamics, the bottom row of Fig. 5 shows the pressure distribution in the ε -neighborhood of the leaflet, that is in the region where the RIIS term is active. While the valve is closed, the whole pressure gradient develops within that region, showing the effectiveness of the RIIS method in providing an obstacle to the flow. Then, while the valve opens, the overall pressure jump between the two sides of the leaflets is relatively small, but non-negligible gradients are present inside the RIIS region: this localized inhomogeneity allows to develop a nonzero leaflet velocity \mathbf{u}_Γ while preserving the incompressibility constraint of Navier-Stokes continuity equation. Indeed, when the valve is fully open and not moving anymore, pressure is essentially constant in the leaflets volume.

4.2 Relevance of the leaflets velocity

As presented in Section 2.1, the RIIS method penalizes a no-slip condition, namely it imposes that the fluid velocity \mathbf{u} must equal the surface velocity \mathbf{u}_Γ

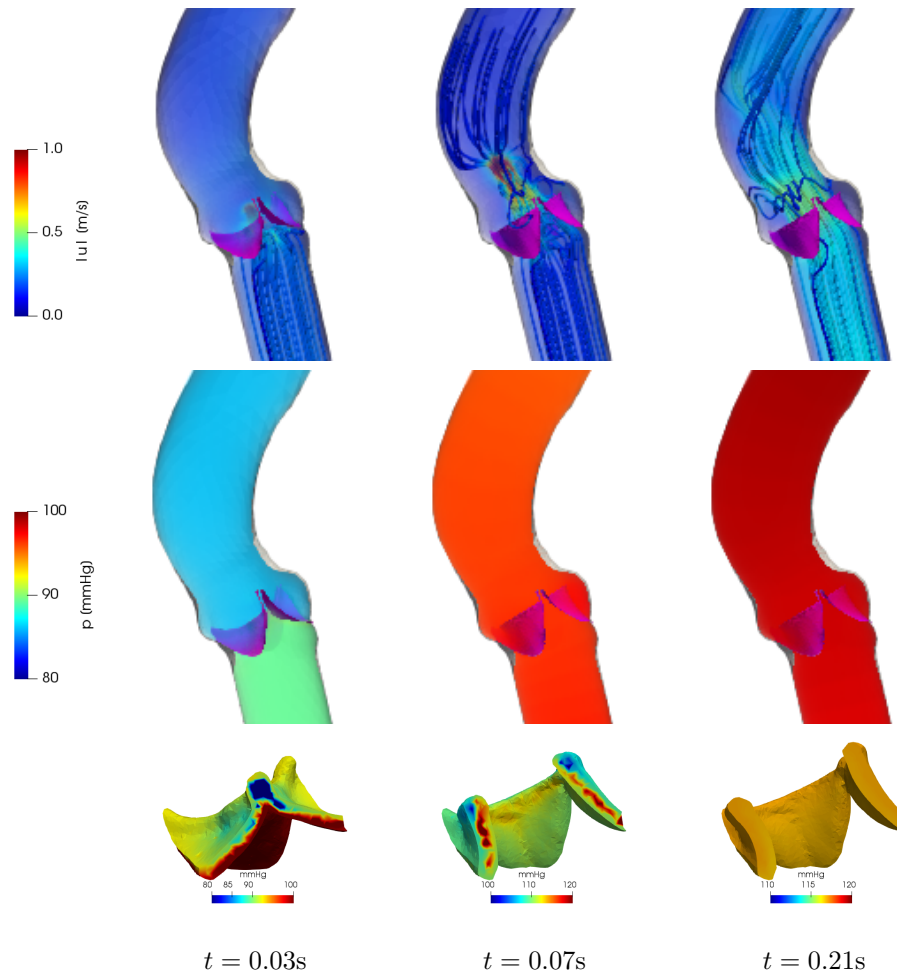


Figure 5: Velocity (above) and pressure distribution in the domain (center) and within the leaflets region (below) under physiological pressure conditions. Valve leaflets are colored in purple.

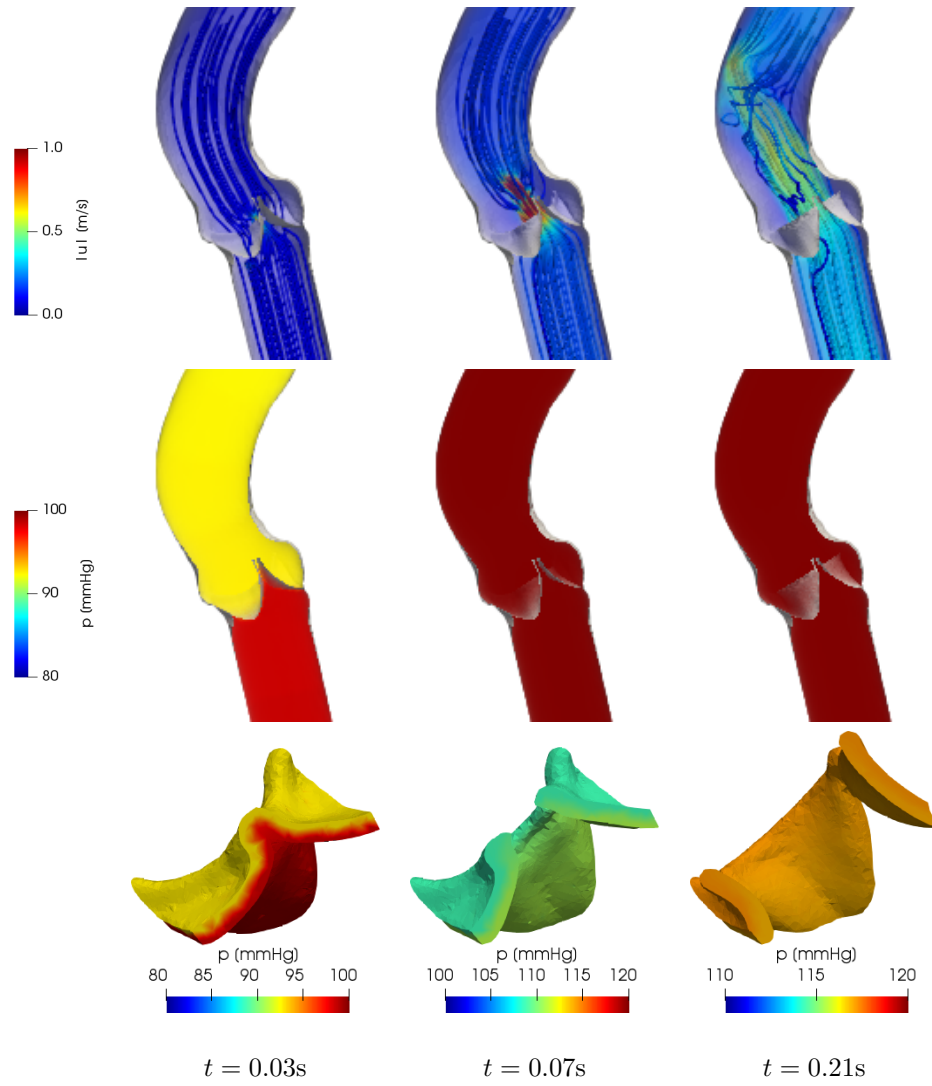


Figure 6: Quasi-static approach $\mathbf{u}_\Gamma = \mathbf{0}$. Velocity (above) and pressure distribution in the domain (center) and within the leaflets region (below) under physiological pressure conditions. Valve leaflets are colored in purple.

in an ε -neighborhood of the immersed surface Γ . Since in the previous works [FFDQ17, FFV⁺20] adopting the RIIS method a quasi-static approach was considered, namely $\mathbf{u}_\Gamma = \mathbf{0}$ was set, we want to discuss the relevance of this velocity in the particular settings described in the previous section. In general, the reconstruction of \mathbf{u}_Γ may instead be more complex, possibly entailing numerical instabilities [FFDQ17]. On the other hand, in the present work the surface velocity is relatively directly derived from the opening coefficient, by expression (10).

In order to observe the effect of the quasi-static approach, a simulation in the same settings and boundary conditions of the previous section is run, the only difference being that $\mathbf{u}_\Gamma = \mathbf{0}$. Resorting to Fig. 4, we can notice that the quasi-static approach entails a much slower opening phase. Moreover, comparing Fig. 6 with Fig. 5 we can notice that a higher pressure jump is developed at the early opening stages, and that a narrower and stronger jet develops in the aorta, non-negligibly impinging the wall in the upper portion of the domain. These results can be motivated by observing that, in order to attain $\mathbf{u} = \mathbf{0}$ in the ε -neighborhood of Γ , the continuous function \mathbf{u} must transition from the flow values to 0 in a surrounding boundary layer, that artificially enlarges the effective obstacle that the leaflets represent to the flow.

We can also compare our results with those of [FFDQ17], in terms of valve opening time. It can be noticed that a much faster opening is observed in that reference (11 ms). This difference is not only in the treatment of the surface velocity \mathbf{u}_Γ , but also in the different valve model considered. We can then state that the model presented in this work represents an improvement in terms of physiological representation of the aortic valve opening.

5 Conclusions

In the present work, a novel reduced model has been introduced for the description of valve dynamics. Starting from a local force balance at the leaflets, considering both flow-induced stress and curvature-based elasticity, as well as damping effects, an ordinary differential equation was derived, governing the evolution of the valve's opening coefficient. Based on this model, a reduced 3D-0D FSI system was proposed, exploiting the RIIS method both to assemble the forcing terms of the 0D valve model, and to account for the valve surface and motion in the blood flow description. This system was employed to simulate the systolic blood flow in the ascending aorta, focusing on the opening phase of the aortic valve. Moreover, a discussion on the relevance of the surface velocity in the employed resistive method was carried out.

The numerical results have shown that the proposed model is suitable for reproducing the aortic valve opening and the associated hemodynamics, with very little additional computational effort: all the additional cost lays in the assembly of the right-hand side of ODE representing the valve dynamics, and this can be done very efficiently. The model also straightforwardly provides an operational definition of the leaflets' velocity \mathbf{u}_Γ , without the need to resorting to complex reconstruction procedures. The comparison with a quasi-static approach as adopted from previous work showed how a proper description of the surface velocity (when available) can have a major impact on the overall dynamics of the system and on the estimation of the aortic jet, at least in some

specific settings.

In order to employ the proposed model in real applications and possibly the study of pathological conditions, different directions of further research may be undertaken. Since the focus of the present work was on the aortic valve’s opening, the investigation may be extended to the whole systole, including the closing stages. Moreover, a sensitivity analysis of the lumped-parameter model response and of the associated hemodynamics w.r.t. the 0D model parameters could help to examine different mechanical properties of the valve, thus opening the way to the study of valvular pathologies such as aortic stenosis or myocarditis-induced leaflet thickening.

6 Acknowledgments

This project has been funded by the European Research Council (ERC) under the European Union’s Horizon 2020 research and innovation programme (grant agreement No 740132, IHEART 2017-2022, P.I. A. Quarteroni).

References

- [AFFL16] F. Alauzet, B. Fabrèges, M. A. Fernández, and M. Landajuela. Nitsche-XFEM for the coupling of an incompressible fluid with immersed thin-walled structures. *Computer Methods in Applied Mechanics and Engineering*, 301:300–335, 2016.
- [AGPT09] M. Astorino, J.-F. Gerbeau, O. Pantz, and K.-F. Traore. Fluid–structure interaction and multi-body contact: application to aortic valves. *Computer Methods in Applied Mechanics and Engineering*, 198(45-46):3603–3612, 2009.
- [AHSG12] M. Astorino, J. Hamers, S. C. Shadden, and J.-F. Gerbeau. A robust and efficient valve model based on resistive immersed surfaces. *International Journal for Numerical Methods in Biomedical Engineering*, 28(9):937–959, 2012.
- [BCC⁺07] Y. Bazilevs, V. Calo, J. Cottrell, T. Hughes, A. Reali, and G. Scovazzi. Variational multiscale residual-based turbulence modeling for large eddy simulation of incompressible flows. *Computer Methods in Applied Mechanics and Engineering*, 197(1-4):173–201, 2007.
- [Bel69] B. Bellhouse. Velocity and pressure distributions in the aortic valve. *Journal of Fluid Mechanics*, 37(3):587–600, 1969.
- [BF⁺10] P. J. Blanco, R. A. Feijóo, et al. A 3d-1d-0d computational model for the entire cardiovascular system. *Computational Mechanics*, eds. E. Dvorking, M. Goldschmit, M. Storti, 29:5887–5911, 2010.
- [BF14] E. Burman and M. A. Fernández. An unfitted Nitsche method for incompressible fluid–structure interaction using overlapping

- meshes. *Computer Methods in Applied Mechanics and Engineering*, 279:497–514, 2014.
- [BGS08] I. Borazjani, L. Ge, and F. Sotiropoulos. Curvilinear immersed boundary method for simulating fluid structure interaction with complex 3d rigid bodies. *Journal of Computational physics*, 227(16):7587–7620, 2008.
- [BGS10] I. Borazjani, L. Ge, and F. Sotiropoulos. High-resolution fluid–structure interaction simulations of flow through a bi-leaflet mechanical heart valve in an anatomic aorta. *Annals of Biomedical Engineering*, 38(2):326–344, 2010.
- [BHK⁺11] Y. Bazilevs, M.-C. Hsu, J. Kiendl, R. Wüchner, and K.-U. Bletzinger. 3D simulation of wind turbine rotors at full scale. Part II: Fluid–structure interaction modeling with composite blades. *International Journal for Numerical Methods in Fluids*, 65(1-3):236–253, 2011.
- [BQČG17] S. Basting, A. Quaini, S. Čanić, and R. Glowinski. Extended ALE method for fluid–structure interaction problems with large structural displacements. *Journal of Computational Physics*, 331:312–336, 2017.
- [CLC04] R. Cheng, Y. G. Lai, and K. B. Chandran. Three-dimensional fluid-structure interaction simulation of bileaflet mechanical heart valve flow dynamics. *Annals of Biomedical Engineering*, 32(11):1471–1483, 2004.
- [dea] <https://www.dealii.org/>.
- [DHPSB03] J. De Hart, G. Peters, P. Schreurs, and F. Baaijens. A three-dimensional computational analysis of fluid–structure interaction in the aortic valve. *Journal of Biomechanics*, 36(1):103–112, 2003.
- [DP15] F. Domenichini and G. Pedrizzetti. Asymptotic model of fluid–tissue interaction for mitral valve dynamics. *Cardiovascular engineering and technology*, 6(2):95–104, 2015.
- [DSGB08] N. D. Dos Santos, J.-F. Gerbeau, and J.-F. Bourgat. A partitioned fluid–structure algorithm for elastic thin valves with contact. *Computer Methods in Applied Mechanics and Engineering*, 197(19-20):1750–1761, 2008.
- [ESH14] D. M. Espino, D. E. Shepherd, and D. W. Hukins. Evaluation of a transient, simultaneous, arbitrary Lagrange–Euler based multi-physics method for simulating the mitral heart valve. *Computer Methods in Biomechanics and Biomedical Engineering*, 17(4):450–458, 2014.
- [FD15] D. Forti and L. Dedè. Semi-implicit BDF time discretization of the Navier-Stokes equations with VMS-LES modeling in a high performance computing framework. *Computers & Fluids*, 117:168–182, 2015.

- [FFDQ17] M. Fedele, E. Faggiano, L. Dedè, and A. Quarteroni. A patient-specific aortic valve model based on moving resistive immersed implicit surfaces. *Biomechanics and Modeling in Mechanobiology*, 16(5):1779–1803, 2017.
- [FFV⁺20] I. Fumagalli, M. Fedele, C. Vergara, L. Dede', S. Ippolito, F. Nicolò, C. Antona, R. Scrofani, and A. Quarteroni. An image-based computational hemodynamics study of the systolic anterior motion of the mitral valve. *Computers in Biology and Medicine*, 123:103922, 2020.
- [FGM08] M. A. Fernández, J.-F. Gerbeau, and V. Martin. Numerical simulation of blood flows through a porous interface. *ESAIM: Mathematical Modelling and Numerical Analysis*, 42(6):961–990, 2008.
- [FVZ18] L. Formaggia, C. Vergara, and S. Zonca. Unfitted extended finite elements for composite grids. *Computers & Mathematics with Applications*, 2018.
- [GLMP09] B. E. Griffith, X. Luo, D. M. McQueen, and C. S. Peskin. Simulating the fluid dynamics of natural and prosthetic heart valves using the immersed boundary method. *International Journal of Applied Mechanics*, 1(01):137–177, 2009.
- [GLSY05] L. Ge, H.-L. Leo, F. Sotiropoulos, and A. P. Yoganathan. Flow in a mechanical bileaflet heart valve at laminar and near-peak systole flow rates: CFD simulations and experiments. *Journal of Biomechanical Engineering*, 127(5):782–797, 2005.
- [GPP97] R. Glowinski, T.-W. Pan, and J. Periaux. A Lagrange multiplier/fictitious domain method for the numerical simulation of incompressible viscous flow around moving rigid bodies:(I) case where the rigid body motions are known a priori. *Comptes Rendus de l'Académie des Sciences-Series I-Mathematics*, 324(3):361–369, 1997.
- [Gri12] B. E. Griffith. Immersed boundary model of aortic heart valve dynamics with physiological driving and loading conditions. *International Journal for Numerical Methods in Biomedical Engineering*, 28(3):317–345, 2012.
- [GS10] L. Ge and F. Sotiropoulos. Direction and magnitude of blood flow shear stresses on the leaflets of aortic valves: is there a link with valve calcification? *Journal of Biomechanical Engineering*, 132(1):014505, 2010.
- [GW08] A. Gerstenberger and W. A. Wall. An extended finite element method/Lagrange multiplier based approach for fluid–structure interaction. *Computer Methods in Applied Mechanics and Engineering*, 197(19-20):1699–1714, 2008.

- [GW10] A. Gerstenberger and W. Wall. An embedded Dirichlet formulation for 3d continua. *International Journal for Numerical Methods in Engineering*, 82(5):537–563, 2010.
- [HH88] T. J. Hughes and G. M. Hulbert. Space-time finite element methods for elastodynamics: formulations and error estimates. *Computer methods in applied mechanics and engineering*, 66(3):339–363, 1988.
- [HHB⁺03] M. Handke, G. Heinrichs, F. Beyersdorf, M. Olschewski, C. Bode, and A. Geibel. In vivo analysis of aortic valve dynamics by transesophageal 3-dimensional echocardiography with high temporal resolution. *The Journal of thoracic and cardiovascular surgery*, 125(6):1412–1419, 2003.
- [HKB⁺14] M.-C. Hsu, D. Kamensky, Y. Bazilevs, M. S. Sacks, and T. J. Hughes. Fluid–structure interaction analysis of bioprosthetic heart valves: significance of arterial wall deformation. *Computational Mechanics*, 54(4):1055–1071, 2014.
- [HLZ15] P. Hansbo, M. G. Larson, and S. Zahedi. Characteristic cut finite element methods for convection–diffusion problems on time dependent surfaces. *Computer Methods in Applied Mechanics and Engineering*, 293:431–461, 2015.
- [JDS96] Z. Jianhai, C. Dapeng, and Z. Shengquan. Ale finite element analysis of the opening and closing process of the artificial mechanical valve. *Applied Mathematics and Mechanics*, 17(5):403–412, 1996.
- [KC90] K. Kunzelman and R. Cochran. Mechanical properties of basal and marginal mitral valve chordae tendineae. *ASAIO transactions*, 36(3):M405–8, 1990.
- [KHS⁺15] D. Kamensky, M.-C. Hsu, D. Schillinger, J. A. Evans, A. Aggarwal, Y. Bazilevs, M. S. Sacks, and T. J. Hughes. An immersogeometric variational framework for fluid–structure interaction: Application to bioprosthetic heart valves. *Computer Methods in Applied Mechanics and Engineering*, 284:1005–1053, 2015.
- [KS06] T. Korakianitis and Y. Shi. Numerical simulation of cardiovascular dynamics with healthy and diseased heart valves. *Journal of biomechanics*, 39(11):1964–1982, 2006.
- [lif] <https://lifex.gitlab.io/lifex>.
- [LLF⁺06] W. K. Liu, Y. Liu, D. Farrell, L. Zhang, X. S. Wang, Y. Fukui, N. Patankar, Y. Zhang, C. Bajaj, J. Lee, et al. Immersed finite element method and its applications to biological systems. *Computer methods in applied mechanics and engineering*, 195(13-16):1722–1749, 2006.

- [Mar15] G. Marom. Numerical methods for fluid–structure interaction models of aortic valves. *Archives of Computational Methods in Engineering*, 22(4):595–620, 2015.
- [MCE⁺14] S. T. Miller, R. Campbell, C. Elsworth, J. Pitt, and D. Boger. An overset grid method for fluid-structure interaction. *World Journal of Mechanics*, 4(07):217, 2014.
- [MDA13] K. L. Moore, A. F. Dalley, and A. M. Agur. *Clinically oriented anatomy*. Lippincott Williams & Wilkins, 2013.
- [MLLR15] A. Massing, M. Larson, A. Logg, and M. Rognes. A Nitsche-based cut finite element method for a fluid-structure interaction problem. *Communications in Applied Mathematics and Computational Science*, 10(2):97–120, 2015.
- [MPGW10] U. M. Mayer, A. Popp, A. Gerstenberger, and W. A. Wall. 3D fluid–structure–contact interaction based on a combined XFEM FSI and dual mortar contact approach. *Computational Mechanics*, 46(1):53–67, 2010.
- [MPH⁺13] G. Marom, M. Peleg, R. Halevi, M. Rosenfeld, E. Raanani, A. Hamdan, and R. Haj-Ali. Fluid-structure interaction model of aortic valve with porcine-specific collagen fiber alignment in the cusps. *Journal of biomechanical engineering*, 135(10):101001, 2013.
- [MYWD07] Y. S. Morsi, W. W. Yang, C. S. Wong, and S. Das. Transient fluid–structure coupling for simulation of a trileaflet heart valve using weak coupling. *Journal of Artificial Organs*, 10(2):96–103, 2007.
- [OF01] S. Osher and R. P. Fedkiw. Level set methods: an overview and some recent results. *Journal of Computational physics*, 169(2):463–502, 2001.
- [Pes72] C. S. Peskin. Flow patterns around heart valves: A numerical method. *Journal of Computational Physics*, 10(2):252 – 271, 1972.
- [RMK14] Y. Rim, D. D. McPherson, and H. Kim. Effect of leaflet-to-chordae contact interaction on computational mitral valve evaluation. *Biomedical engineering online*, 13(1):31, 2014.
- [RSA⁺20a] F. Regazzoni, M. Salvador, P. C. Africa, M. Fedele, L. Dede’, and A. Quarteroni. A cardiac electromechanics model coupled with a lumped parameters model for closed-loop blood circulation. Part I: model derivation, 2020. arXiv:2011.15040 [math.NA].
- [RSA⁺20b] F. Regazzoni, M. Salvador, P. C. Africa, M. Fedele, L. Dede’, and A. Quarteroni. A cardiac electromechanics model coupled with a lumped parameters model for closed-loop blood circulation. Part II: numerical approximation, 2020. arXiv:2011.15051 [math.NA].

- [SCM⁺07] S. Schievano, L. Coats, F. Migliavacca, W. Norman, A. Frigiola, J. Deanfield, P. Bonhoeffer, and A. M. Taylor. Variations in right ventricular outflow tract morphology following repair of congenital heart disease: implications for percutaneous pulmonary valve implantation. *Journal of cardiovascular magnetic resonance*, 9(4):687–695, 2007.
- [SDHBVdV04] J. Stijnen, J. De Hart, P. Bovendeerd, and F. Van de Vosse. Evaluation of a fictitious domain method for predicting dynamic response of mechanical heart valves. *Journal of Fluids and Structures*, 19(6):835–850, 2004.
- [SZRM20] J.-H. Seo, C. Zhu, J. Resar, and R. Mittal. Flow physics of normal and abnormal bioprosthetic aortic valves. *International Journal of Heat and Fluid Flow*, 86:108740, 2020.
- [TS03] T. Tezduyar and S. Sathe. Stabilization parameters in SUPG and PSPG formulations. *Journal of Computational and Applied Mechanics*, 4(1):71–88, 2003.
- [TS07] T. E. Tezduyar and S. Sathe. Modelling of fluid–structure interactions with the space–time finite elements: solution techniques. *International Journal for Numerical Methods in Fluids*, 54(6-8):855–900, 2007.
- [TTTS18] K. Takizawa, T. E. Tezduyar, T. Terahara, and T. Sasaki. Heart valve flow computation with the space–time slip interface topology change (ST-SI-TC) method and isogeometric analysis (IGA). In *Biomedical Technology*, pages 77–99. Springer, 2018.
- [vLAvdV06] R. van Loon, P. D. Anderson, and F. N. van de Vosse. A fluid–structure interaction method with solid-rigid contact for heart valve dynamics. *Journal of Computational Physics*, 217(2):806–823, 2006.
- [VLS⁺13] E. Votta, T. B. Le, M. Stevanella, L. Fusini, E. G. Caiani, A. Redaelli, and F. Sotiropoulos. Toward patient-specific simulations of cardiac valves: state-of-the-art and future directions. *Journal of Biomechanics*, 46(2):217–228, 2013.
- [Wig23] C. J. Wiggers. *Modern aspects of the circulation in health and disease*. Lea & Febiger, 1923.
- [WZK⁺18] M. C. Wu, R. Zakerzadeh, D. Kamensky, J. Kiendl, M. S. Sacks, and M.-C. Hsu. An anisotropic constitutive model for immersed-geometric fluid–structure interaction analysis of bioprosthetic heart valves. *Journal of Biomechanics*, 74:23–31, 2018.
- [YYKZ18] J. Yang, F. Yu, M. Krane, and L. T. Zhang. The perfectly matched layer absorbing boundary for fluid–structure interactions using the immersed finite element method. *Journal of fluids and structures*, 76:135–152, 2018.

- [ZSJ09] F. Zahle, N. N. Sørensen, and J. Johansen. Wind turbine rotor-tower interaction using an incompressible overset grid method. *Wind Energy: An International Journal for Progress and Applications in Wind Power Conversion Technology*, 12(6):594–619, 2009.
- [ZVF18] S. Zonca, C. Vergara, and L. Formaggia. An unfitted formulation for the interaction of an incompressible fluid with a thick structure via an XFEM/DG approach. *SIAM Journal on Scientific Computing*, 40(1):B59–B84, 2018.
- [Zyg14] Zygote Media Group, Inc. Zygote solid 3D heart generation II development report. Technical report, 2014.